Total RNA isolation from hepatic cells was performed using a Nucleospin RNA II kit (Macherey-Nagel GmbH & Co. KG, Düren, Germany) according to the manufacturer's protocol, and the genomic DNA was eliminated via DNase I digestion. cDNA synthesis from the extracted RNA (1 μg) was performed using a High Capacity cDNA Reverse Transcription kit with random hexamers (Life Technologies), as described previously.[19] cDNAs for the standard curves were also synthesized from each hENT1 mRNA isoform at different copy numbers [1, 5, 25, 50, 100, 250 copies ($\times 10^3$)].

Quantitative real-time polymerase chain reaction (qPCR)

The expression levels of the hENT1 mRNA isoforms in human hepatocytes and hepatoma cells were analyzed by a SYBR green-based qPCR method using specific primers for total hENT1 mRNA, as well as hENT1a1 mRNA, all hENT1b mRNA isoforms, all hENT1c mRNA isoforms, and all hENT1d mRNA isoforms (hereafter referred to as hENT1b, hENT1c, and hENT1d, respectively), as shown in Table s2. The primer positions were also depicted in Fig. 1. The glyceraldehyde 3-phosphate dehydrogenase (GAPDH) mRNA expression level was also determined. The specific amplification was confirmed by DNA sequencing. The expression levels of hENT1 mRNA isoforms were normalized using the GAPDH mRNA expression level. In addition, hENT1a1, hENT1c, and hENT1d mRNA copy numbers (copies/μg total RNA) were determined using the standard curves, which were generated using standard cDNAs prepared from *in vitro* transcribed hENT1 mRNA isoforms.

RNA ligase-mediated 5'-rapid amplification of cDNA ends (RLM-5'-RACE) and reverse-transcriptase PCR (RT-PCR)

RLM-5'-RACE was performed using a GeneRacer RLM-RACE Kit (Life Technologies) according to the manufacturer's protocol. Total RNA was extracted from HH187 and HepG2 cells, followed by ligation to the RNA adaptor at the 5'-end of intact mRNA. After reverse transcription, the first RT-PCR was performed using specific primers for hENT1c, hENT1d, or the adaptor (Table s2). Subsequently, the nested PCR was performed using different primer sets (Table s2, Fig. 1), after which the products were applied to DNA sequence analysis.

RT-PCR for detection of hENT1c and 1d mRNA isoforms expression was performed using primer sets that were designed to span an exon α (Table s2 and Fig. 1).

Short-hairpin RNA (shRNA)-mediated knockdown of hENT1d mRNA

In order to archive an isoform-specific mRNA knockdown, it is necessary to design an

RNAi target sequence within the 5'-UTR region of each mRNA isoform. Based on this requirement, an hENT1d mRNA-specific shRNA sequence was identified using the Target Sequence Selector (Clontech, Mountain View, CA) (http://bioinfo.clontech.com/rnaidesigner/sirnaSequenceDesignInit.do). However, due to the intrinsic sequence characteristics of the 5'-UTR of the hENT1c mRNA, we were unable to design a specific hENT1c mRNA sequence using the same program or with another RNAi sequence design program (Life Technologies). Accordingly, only the hENT1d mRNA could be applied to the isoform-specific knockdown experiment.

The shRNA target sequence for hENT1d mRNA knockdown (dKD-shRNA, Table s2 and Fig. 1) and the scramble shRNA sequence (control-shRNA, of which sequence information was obtained from Sigma, Table s2) were independently inserted into the RNAi-Ready pSIREN-RetroQ Vector (Clontech). DNA sequencing was performed to confirm the resulting vectors (dKD/pSIREN and control/pSIREN).

The retroviral vectors of dKD-shRNA and control-shRNA were prepared using the dKD/pSIREN and the control/pSIREN according to the manufacturers' protocols (Takara Bio and Life Technologies). Briefly, these pSIREN vectors were separately transfected into 293FT cells with a Retrovirus Packaging Kit Ampho (Takara Bio) using Lipofectamine2000 (Life Technologies). The virus was collected from the culture medium and concentrated using the Retro-X Concentrator (Clontech).

The retrovirus vectors were then separately transduced into HepG2 cells, and the shRNA-expressing cells, which were respectively named dKD-HepG2 cells or control-HepG2 cells, were selected using puromycin treatment (Wako, Osaka, Japan). The cDNA synthesis and qPCR methods were described above.

Transient transfection and luciferase reporter gene assay

Transient transfection and luciferase reporter gene assays were performed primarily via the previously described methods.[19] Preparation of pGL4.17 firefly luciferase reporter plasmids (Promega, Madison, WI) containing the P1 promoter region (-1883/+143), the P2 promoter region (-2000/+29, previously referred to as P2.1), or the P3 promoter region (-1945/+141) was described in the previous study.[19] pGL4.70 *renilla* luciferase reporter plasmids (Promega) were used as an internal control.

One of the reporter plasmids (or the empty pGL4.17 vector), together with pGL4.70 vector, were transfected into HepG2 cells, Huh-7 cells, or FLC-7 cells using Lipofectamine LTX (Life Technologies). The results are expressed as a relative ratio (firefly/*renilla*) of luciferase activities.

Chromatin immunoprecipitation (ChIP) assay

Chromatin immunoprecipitation assays were performed in HepG2 cells and FLC7 cells using a ChIP-IT kit (Active Motif, Carlsbad, CA) according to the manufacturer's protocol. Sheared chromatin was prepared from cross-linked cells using a sonicator. Magna ChIP protein G magnetic beads (Millipore, Bedford, MA), which had been blocked with ssDNA/BSA (2.5 mg/mL salmon sperm DNA (Wako) and 2.5 mg/mL bovine serum albumin (Sigma) for 2 hr, were pre-incubated with the sheared chromatin (20 μg) for 1 hr. The cleaned chromatin was incubated with ssDNA/BSA and proteinase inhibitors, followed by incubation with either anti-histone H3 acetylated lysine 9 (H3K9ac) (Millipore, 07-352) antibodies (2.5 μL), anti-histone H3 antibodies (3 μg, ab1791, Abcam, Cambridge, UK) or normal rabbit IgG (3 μg, Santa Cruz Biotechnology, Santa Cruz, CA) for 14 hr. The magnetic beads, which had been blocked with the ssDNA/BSA, were then added to the mixture and incubated for 3 hr. DNA fractions were recovered from the precipitated beads using conventional reverse cross-linking, proteinase K treatment, and DNA purification methods. "Input DNA" was also prepared from chromatin using the same treatments, except for immunoprecipitation.

A SYBR green-based qPCR method was used for quantification of precipitated DNA amounts of the P1 and P2 promoters or the 3'-intergenic region (2723 bp downstream from translation stop codon). A fluorescence probe-based qPCR was used for detection of the P3 promoter region, in which the UPL universal probe #57 (Roche Diagnostics, Basel, Switzerland) was used. Specific primers are shown in Table s2 and Fig. 1. Values are represented as fold enrichment calculated with the following formula: $2^{\wedge\Delta Ct(H)}$-$2^{\wedge\Delta Ct(IgG)}$, where $\Delta Ct_{(H)}$ = Ct(input) – Ct (Histone antibodies) and $\Delta Ct_{(IgG)}$ = Ct(input) – Ct (normal IgG). Next, the values of H3K9ac were normalized for the value obtained from the unmodified histone H3 antibodies (H3K9ac/H3).

Sequence analysis

The numbers of the G and C nucleotides along with the number of CpG dinucleotides (CpG) in each promoter region (-500/+500, where +1 indicated the position of the most upstream transcription start site in the region) were counted. The normalized CpG content in the promoter region was represented as the ratio of the observed over the expected CpGs, which was determined using the following equation: Normalized CpG = Observed CpGs/[(Observed Gs+Cs)/2][2].[20,21] *Cis*-elements embedded in the promoter region were predicted using the JASPAR database [Portales-Casamar E, Thongjuea S, Kwon AT, Arenillas D, Zhao X, Valen E, Yusuf D, Lenhard B, Wasserman WW, and Sandelin A (2010) JASPAR 2010: the greatly expanded open-access database of transcription factor binding profiles. Nucleic Acids Res 38: D105-110. http://jaspar.genereg.net/].

Prediction of mRNA secondary structure (the regions containing 5'-UTR, exon 1, and exon 2 of each isoform) was performed using a computer program (CentroidFold, http://www.ncrna.org/) [Sato K, Hamada M, Asai K, and Mituyama T (2009) CENTROIDFOLD: a web server for RNA secondary structure prediction. Nucleic Acids Res 37: W277-280]. When searching the upstream open reading frame (uORF) in 5'-UTR, the Kozak sequence gccRccAUGG was taken into consideration.[22)]

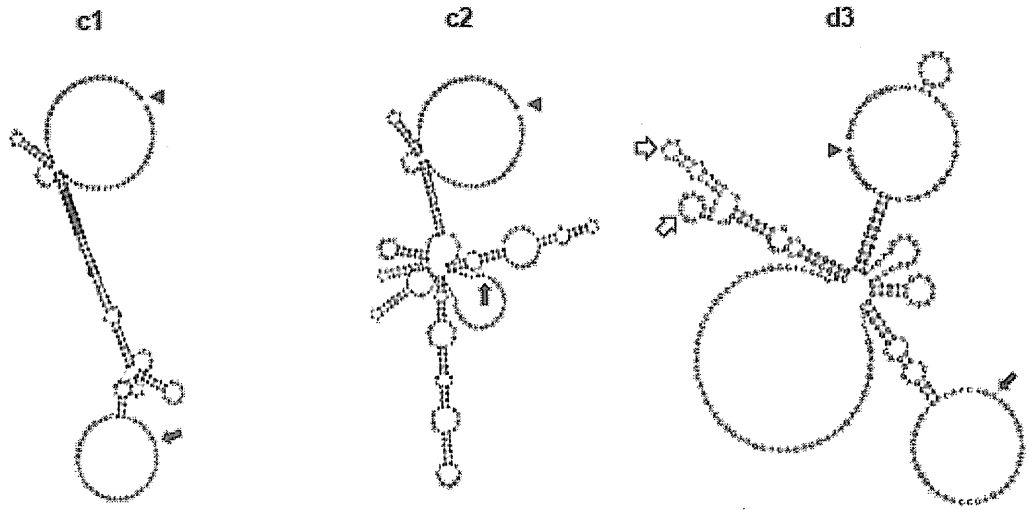

Fig. s1. Prediction of the secondary structure of 5'-UTR of hENT1c1, c2, and d3 mRNA.
The secondary structure of 5'-UTR, together with exons 1 and 2, of hENT1c1, c2, and d3 mRNA were predicted using the CentroidFold (http://www.ncrna.org/). The complexity was indicated by folding energy (65, 99 and 75 kcal/mol for c1, c2, and d3 5'-UTR, respectively). The uORF was searched based on the assumption that it starts with ATG having high homology to the Kozak sequence and ends with TGA/TAG/TAA. Arrowheads indicate the first nucleotide of mRNA, while closed arrows indicate the translational start codon for mature hENT1 protein. Open arrows indicate the start codons for uORFs. Deduced amino acids length for the first and the second uORFs are 6 and 46, respectively.

Table s1 Donor characteristics

	HH187	HH268	HH291	HH283	HH225	HH229	HH314	HH278
Basic donor information[a]								
Age	50	54	69	53	42	56	53	68
Race	N/A	C	C	C	C	A	AA	C
Sex	F	F	F	M	M	M	M	M
COD	N/A	CVA	CVA	CVA	CVA	CVA	CVA	CVA
Serologies[b]								
Hepatitis B sAG	N	N	N	N	N	N	N	N
Anti-Hepatitis B core	N	N	N	N	N	N	N	N
Anti-Hepatitis C	N	N	N	N	N	N	N	N
RPR/STS	N/A	N	N	N	N	N	N	N
Anti-CMV	N/A	P	P	P	N	P	N	P
Anti-HTLV1/2	N/A	N	N	N	N	N	N	N
Past Medical History[c]								
Respiratory Disease	N/A	No	No	No	asthm	No	No	emphyse
Neurological Disease	N/A	CVA	No	No	a	No	No	ma
Cancer	Yes	No	No	No	Yes	No	No	No
Diabetes	No	IDDM	No	No	No	No	No	No
Hypertension	N/A	Yes	N/A	No	Yes	No	No	No
Liver Disease	Metasta	No	No	No	Yes	No	No	Yes
GI Disease	sis	No	No	No	No	No	No	No
Kidney Disease	N/A	RI	No	No	No	Yes	No	No
Smoking	N/A	No	Yes	Yes	No	No	Yes	No
Alcohol	Yes	Yes	Yes	Yes	Yes	rarel	Yes	Yes
Drug Use	N/A	No	No	No	Yes	y	Yes	Yes
	Yes				No	No		No

[a], C, Caucasian; F, female; M, male; CVA, cerebrovascular accident; N/A, not available.

[b], N, negative; P, positive; N/A, not available.

[c], IDDM, insulin-dependent diabetes mellitus; RI, renal insufficiency; N/A, not available.

Table s2 Primers and oligonucleotides used in this study

Assay name	Primer name	Sequence (5' > 3')
qPCR		
	hENT1a-U	GCTGGGTGGGGGTCAAGTT
	hENT1a-L	AACAGGCCAGTGGAGGAGT
	hENT1b-all U	GGAGCCTGAGGACCCTGCG
	hENT1b-all L	TGCCCCTTGCGGAGGTCAAC
	hENT1c-all U	AGGGAAGCTGCAGCGAGA
	hENT1c-all L	GCCGCAGAAGCACTGCTC
	hENT1d-all U	TGCGCTCTCCAGCTGTGG
	hENT1d-all L	TGCGGGCCCCTAGTTCTC
	ENT1 total U-qRT	AGCCAGGGAAAACCGAGA
	ENT1 total L-qRT	ACCCAGCATGAAGAAGATAAGC
	GAPDH-U	AGCCACATCGCTCAGACAC
	GAPDH-L	GCCCAATACGACCAAATCC
RT-PCR		
	hENT1c-rt-U	GCGGGAGAGGGAAGCTGC
	hENT1d-rt-U	GGGCTGCGCTCTCCAGCTGTGGCTATGG
	hENT1c/d-rt-L	CGCCTGGGCGTCCTTGCTCAGTTCAGCA
RLM-5'-RACE		
	RACE-1st-F	CGACTGGAGCACGAGGACACTGA
	hENT1cRACE-1st-L	GCCGCAGAAGCACTGCTC
	hENT1dRACE-1st-L	GGACTTGGTGGGGGACGGAA
	RACE-2nd-F	GGACACTGACATGGACTGAAGGAGTA
	hENT1cRACE-2nd -L	CTGCAGCTTCCCTCTCCCGC
	ENT1dRACE- 2nd -L	ATCTCGGGGCTGGGGCCATA
ChIP-qPCR		
	P1-U	GGGAGCCAGGTAGAGTCTGAGC
	P1-L	CCCCTCAGGACGACTCAACTT
	P2-U	CAGCGGAGGGCGGGTTTGAATG
	P2-L	CAGCACCTGCCGCAGAAGCACT
	P3-U	GCCTGTTGCAGCCTCTCTT
	P3-L	TTCTCTCCCTCCTCATCTCG
	3'-F	ACTTGCTGCTGGTCATCACCTTC
	3'-R	CAAGAGGGACATTCCTGTGTTGC
cDNA cloning		

hENT1a-U+XhoI	CATACTCGAGTCACCATGACAACCAGTCACCAGC
hENT1c1-U	GTAGAACCAGGGGTTTGAATGTGC
hENT1c1-U+NheI	CTAGCTAGCGGGGTTTGAATGTGC CCC
hENT1d3-U+NheI	CTAGCTAGCACACCGGTCAGGCCC GGC
hENT1-L	AGTGGAGAAACTCAAGCAAATGCC
hENT1-L+EcoV	ACGTGATATCTCACACAATTGCCCGGAACAGGAA

shRNA

scramble-shRNA[a]	GATCCCAACAAGATGAAGAGCACCAACTGTGAA GCCACAGATGGGTTGGTGCTCTTCATCTTGTTGTTT TTTA
1d specific-shRNA[a]	GATCCATGCTCACTCCAAAGTCTCACTGTGAAGCCA CAGATGGGTGAGACTTTGGAGTGAGCATTTTTTTA

[a], the sense strand sequence is shown. The underline indicates the scramble RNAi target sequence that contains four mismatches to any known human or mouse genes, which is provided by Sigma. The double underline indicates the target RNAi sequence for all hENT1d mRNA isoforms, which was designed using the Target Sequence Selector (Clontech, Mountain View, CA) (http://bioinfo.clontech.com/rnaidesigner/sirnaSequenceDesignInit.do).

Drug Metab. Pharmacokinet. 29 (2): 211–214 (2014).

Note

Functional Analysis of Purine Nucleoside Phosphorylase as a Key Enzyme in Ribavirin Metabolism

Tomomi FURIHATA*, Satoshi KISHIDA, Hanae SUGIURA, Atsuko KAMIICHI, Minami IIKURA and Kan CHIBA

Laboratory of Pharmacology and Toxicology, Graduate School of Pharmaceutical Sciences, Chiba University, Chiba, Japan

Full text and Supplementary materials of this paper are available at http://www.jstage.jst.go.jp/browse/dmpk

Summary: Ribavirin is a purine nucleoside analogue that possesses potent anti-hepatitis C virus activity, and it has long been considered likely that ribavirin undergoes a first-pass metabolism at the small intestine. Although purine nucleoside phosphorylase (PNP) is assumed to be involved in this metabolism, this has not been conclusively demonstrated. Furthermore, no pharmacogenomic studies related to PNP-mediated ribavirin phosphorolysis have previously been conducted. In this study, we sought to identify the role of PNP in ribavirin phosphorolysis in the human small intestine, and to clarify the effect of the single nucleotide polymorphism (rs1049564) on PNP's ribavirin phosphorolysis activity. The results of our investigations show that PNP is abundantly expressed in the human small intestine, and that intestinal ribavirin phosphorolysis is severely inhibited by ganciclovir, a PNP-inhibitor. Therefore, PNP is likely to play a primary role in the ribavirin phosphorolysis in the human small intestine. On the other hand, the results of our attempt to clarify the function of rs1049564 show that it does not affect PNP's ribavirin phosphorolysis activity. We believe that the present study will facilitate further pharmacogenomic and biochemical characterization of PNP as a key metabolic enzyme of ribavirin.

Keywords: chronic hepatitis C; phosphorolysis; purine nucleoside phosphorylase; ribavirin; single nucleotide polymorphism; small intestine; $TCONH_2$

Introduction

Ribavirin (1-β-D-ribofuranosyl-1H-1,2,4-triazole-3-corboxamide) is a purine nucleoside analogue that shows potent anti-hepatitis C virus activity, and has thus been a key component of chronic hepatitis C treatment regimens.[1] The 5′-phospate derivatives of ribavirin, which are its pharmacologically active forms, have been found to accumulate in cells at significant levels. Earlier reports have shown that higher extracellular ribavirin concentrations can be associated with higher ribavirin accumulation levels along with higher antiviral activity levels *in vitro*.[2] Furthermore, clinical observation has shown that higher ribavirin plasma concentrations are associated with better therapeutic responses.[3] Thus, it appears likely that the factors governing ribavirin's plasma concentrations play a pivotal role in treatment success.

Previous pharmacokinetic studies have provided results showing that the urinary excretion rate of intravenously administered ribavirin is much higher than that after oral administration, while the excretion rate of 1,2,4-triazole-3-carboxamide ($TCONH_2$), a primary metabolite of ribavirin, shows the opposite behavior, which suggests that ribavirin undergoes a first-pass metabolism.[4] Based on the results obtained so far, the small intestine is believed to play an important role in this first-pass metabolism.[1] Furthermore, because such first-pass metabolism levels appreciably affect the extent of bioavailability (from 28% to 85% among individuals),[5] it is important to identify the responsible enzyme(s) along with the factors contributing to their functional variability in the small intestine. These, for the most part, remain undetermined.

The metabolism of ribavirin to $TCONH_2$ occurs in a manner similar to the endogenous purine nucleoside phosphorolysis in which purine nucleoside phosphorylase (PNP) is exclusively involved. PNP is a ubiquitously-expressed enzyme that plays a pivotal role in the purine salvage pathway.[6] In the presence of an inorganic orthophosphate used as a second substrate, it breaks

Received June 12, 2013; Accepted September 23, 2013
J-STAGE Advance Published Date: October 8, 2013, doi:10.2133/dmpk.DMPK-13-NT-065
**To whom correspondence should be addressed:* Tomomi FURIHATA, Ph.D., *Laboratory of Pharmacology and Toxicology, Graduate School of Pharmaceutical Sciences, Chiba University, 1-8-1 Inohana, Chuou-ku, Chiba 260-8675, Japan. Tel. +81-43-226-2894, Fax. +81-43-226-2894, E-mail: tomomif@faculty.chiba-u.jp*
This work was supported by a grant (22790145) from the Ministry of Education, Sciences, Sports and Culture of Japan and partially supported by a Grant-in-Aid for Scientific Research (Emergency Research Project to Conquer Hepatitis) from the Ministry of Health, Labor and Welfare, Japan, and a research grant from the Gout Research Foundation (Tokyo, Japan).

down the glycosidic bond of purine nucleoside (primarily inosine and guanosine in humans) to produce the purine base and ribose-(deoxyribose)-1-phosphate. Based on the nature of PNP, it was felt that a more detailed examination into the ways that human PNP impacts ribavirin's phosphorolysis activity, and thus its pharmacokinetic behavior, would be a constructive endeavor.[7] However, prior to this study, the question as to whether PNP is involved in ribavirin phosphorolysis in the human small intestine had yet to be explored. Additionally, no pharmacogenomic study of PNP regarding ribavirin metabolism had yet been performed.

In this report, we provide results that show the important role of PNP in ribavirin phosphorolysis in the human small intestine. We also show the results of a functional analysis of the single nucleotide polymorphism (SNP) in the *PNP* gene (p.G51S, rs1049564), which has demonstrated a relatively high allelic frequency, has been associated with cognitive decline in Alzheimer's disease patients, and has been associated with arsenic toxicity.[8,9]

Methods

Human samples: Pooled human jejunal S9 and pooled human liver cytosol were obtained from KAC (Kyoto, Japan) and BD Bioscience (Woburn, MA), respectively. The human jejunal cytosol was prepared from the S9 sample using a centrifugation method. The use of human samples in this study was approved by the Ethics Committee of the Graduate School of Pharmaceutical Sciences, Chiba University.

Purified PNP and PNP p.G51S preparation: PNP cDNA was cloned from human small intestine cDNA and inserted into the *Escherichia coli* (*E. coli*) expression vector pET-14b (Novagen, Madison, WI) in order to generate PNP/wt/pET. PNP cDNA harboring the SNP rs1049564 was generated by inverse-PCR, resulting in PNP/p.G51S/pET.

PNP/wt and PNP/p.G51S production in *E. coli* was separately performed essentially according to the manufacturer's protocol (Novagen). PNP/wt and PNP/p.G51S were purified from each soluble fraction using a HisTALON Gravity Columns kit (Clontech, Mountain View, CA) according to the manufacturer's protocol. The His-tag of the purified protein was removed by thrombin treatment.

PNP activity determination: Inosine phosphorylase activity of purified PNPs or human tissue cytosols was determined using the colorimetric analysis method. The ribavirin phosphorylase activity of the purified PNPs or human tissue cytosols was examined by determining the amount of $TCONH_2$ using a high-performance liquid chromatography system. A calibration curve (0 to 10 μM) was generated using the authentic $TCONH_2$ (Tokyo Kasei, Tokyo, Japan). Ganciclovir (a known PNP inhibitor)[6] (3 mM, Sigma, St. Louis, MO), thymidine (a substrate of thymidine phosphorylase and, to a lesser extent, uridine phosphorylase) (0.5 mM, Sigma), and inosine (0.5 mM) were used in an inhibition assay. For each analysis, substrate concentrations are indicated in the figure legends.

Specific inosine or ribavirin phosphorylase activity of PNP was expressed in terms of the amount of substrate metabolized in one minute under specified conditions. Enzyme kinetic parameters were estimated using a computer program (DeltaGraph Ver 4.5, SPSS Inc., Chicago, IL), which is designed for non-linear regression analysis.

Western blotting analysis: Purified PNPs (0.1 μg each) or human tissue cytosols (40 μg each) were separated by sodium dodecyl sulfate–polyacrylamide gel electrophoresis and transferred to a nitrocellulose membrane. After blocking with 5% skim milk, the membrane was incubated with either anti-PNP polyclonal antibodies (Abnova, Taipei, Taiwan) or anti-β actin antibodies (Sigma), followed by anti-mouse IgG antibodies (Sigma). The chemiluminescence was detected by LAS-1000 plus (Fuji Film, Tokyo, Japan).

Others: Method details, including other methods utilized, are provided in the supplemental materials.

Results

Ribavirin metabolic profile in the human small intestine cytosol and the human liver cytosol: To examine PNP expression in the human small intestine, Western blotting analysis was performed. The human liver cytosol was used as a comparison. The results showed that PNP expression was detected in both tissues, but the expression level in the small intestine was apparently higher than that in the liver (**Fig. 1A**). Next, the ribavirin phosphorolysis properties of these tissue cytosols were examined. Consistent with the PNP protein levels, the ribavirin phosphorolysis activity level of the small intestine was found to be significantly higher than that of the liver (**Fig. 1B**). This was also the case with the inosine phosphorylase activity level (**Supplemental Fig. s1**). Unexpectedly, we found that the reaction kinetic

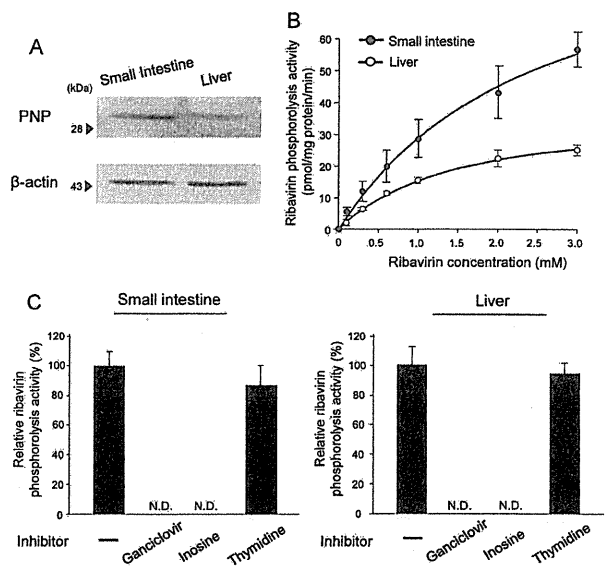

Fig. 1. Contribution of PNP to ribavirin metabolism in the human small intestine and the liver

A: PNP protein expression in the human small intestine and the liver was examined by Western blotting analysis. Each tissue cytosol (40 μg) was loaded on the gel in a separate lane. PNP protein was detected using anti-PNP antibodies, and β-actin protein expression was used as a loading control. B: Ribavirin phosphorolysis activity in the human small intestine (black circles) and the liver (white circles) was determined. Ribavirin concentrations were 0, 100, 300, 600, 1,000, 2,000, and 3,000 μM, and inorganic orthophosphate concentration was set to 50 mM. Each activity value is expressed as mean ± S.D. (pmol/mg protein/min) for three independent determinations, each performed in duplicate. C: The contribution of PNP to ribavirin phosphorolysis (2,000 μM) in the small intestine and in the liver was examined using ganciclovir (an inhibitor of PNP) (3 mM), inosine (0.5 mM) and thymidine (0.5 mM). The relative activity value in the absence of the inhibitor was set to 100%. Each value is the mean ± S.D. of relative activity for three independent experiments, each performed in duplicate. N.D., not detected.

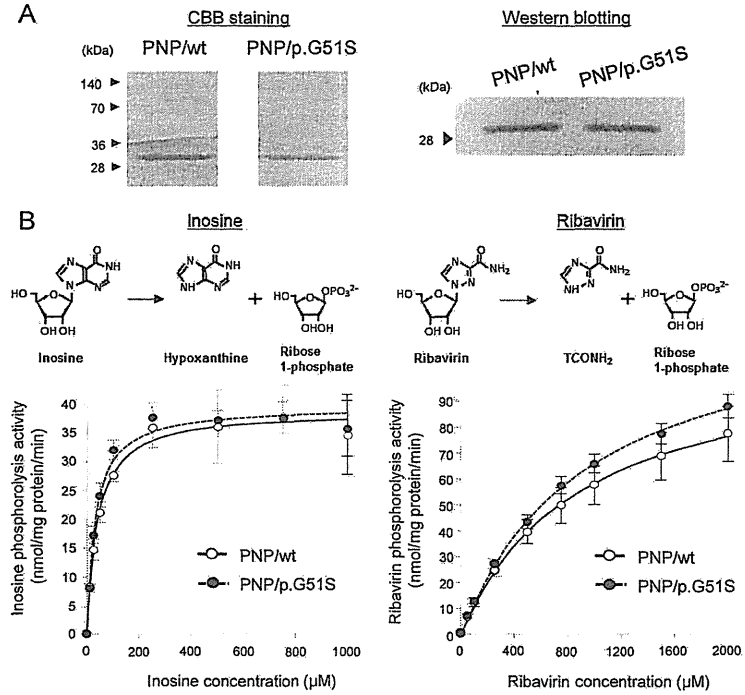

Fig. 2. Examination of effect of the SNP p.G51S on phosphorolysis activity of PNP
A: Purification of PNP/wt and PNP/p.G51S from *E. coli.* was confirmed by SDS-PAGE coupled with Coomassie Brilliant Blue staining (left) and by Western blotting analysis using anti-PNP antibodies (right). B: Inosine (left) or ribavirin (right) phosphorolysis activities of purified PNP/wt (white circles) and PNP/p.G51S (black circles) were determined. Inosine concentrations were 0, 10, 25, 50, 100, 250, 500, 750, and 1,000 μM. Ribavirin concentrations were 0, 50, 100, 250, 500, 750, 1,000, 1,500 and 2,000 μM. The inorganic orthophosphate concentration was 50 mM for both activity determinations. Each value is expressed as mean ± S.D. (nmol/mg protein/min) for three independent determinations, each performed in duplicate.

profiles were different between the two tissues (**Supplemental Table s1**). Although the reason for these differences was unclear, they might be related to differential post-transcriptional modifications of PNP (further explanation can be found in the **Supplemental materials**).

To clarify the involvement of PNP in ribavirin phosphorolysis in the human tissues, an inhibition assay was performed using ganciclovir,[6] inosine, and thymidine. The results showed that the ribavirin phosphorolysis activities in the small intestine and the liver could be completely inhibited by either ganciclovir or inosine, but thymidine did not significantly affect the activities in either tissue (**Fig. 1C**).

Production of recombinant PNP/wt and PNP/p.G51S and their inosine and ribavirin phosphorolysis activities: Purified PNP/wt and PNP/p.G51S were obtained using the *E. coli* expression system to examine effect of the SNP on its function. Both purified PNPs showed the expected molecular size along with immunoreactivity against anti-PNP antibodies (**Fig. 2A**). The results showed that both PNP/wt and PNP/p.G51S possessed high phosphorylase activity levels toward inosine and ribavirin (**Fig. 2B**). The kinetic parameters of these activities were found to be comparable with one another (**Supplemental Table s1**), suggesting that this SNP did not affect the catalytic property of PNP for inosine or ribavirin phosphorolysis.

Discussion

Here we first show ribavirin phosphorolysis activity in the human small intestine. We found that PNP is very likely to be responsible for this phosphorolysis based on the results showing that PNP can catalyze ribavirin phosphorolysis, that PNP is abundantly expressed in the small intestine, and that the intestinal ribavirin phosphorolysis is severely inhibited by ganciclovir and inosine, but not thymidine. Although the possible involvement of other nucleoside metabolism enzymes in ribavirin phosphorolysis cannot be fully ruled out, our results show strong support for the thought that ribavirin's first-pass metabolism primarily occurs in the small intestine, and therefore, it is considered likely that PNP plays a key role in the first-pass metabolism that affects the ribavirin absorption level.

The importance of intestinal PNP in ribavirin metabolism could be further underscored in *in vivo* conditions. It has been reported that, in order to efficiently catabolize dietary purine nucleosides, PNP is specifically co-localized with other purine catabolic enzymes, such as xanthine oxidase, at the brush border/apical portion of enterocytes, where a purine/ribavirin uptake transporter (concentrative nucleoside transporter 2, CNT2) also exists.[10,11] Therefore, it is probable that a functional linkage among purine transporter/enzymes remarkably enhances the purine nucleoside catabolism level to the extent that most dietary purine nucleosides are broken down into their metabolites, which has been noted in rat and human intestinal cells.[12,13] Accordingly, we speculate that ribavirin could also be efficiently metabolized *via* this transport/enzyme complex in enterocytes. Furthermore, since it has been reported that nucleosides transported by CNTs are more likely to be converted to the corresponding nucleobases than those transported by facilitative transporters in kidney tubular cells,[14] this

might have some relation to the speculation.

In addition to the phosphorolysis pathway, it is well known that ribavirin is intracellularly metabolized to its phosphorylated forms by adenosine kinase or other nucleotide kinases. Therefore, although we have yet to perform any experiments related to this issue, it should at least be mentioned that ribavirin phosphorylation in the small intestine might have a significant impact on ribavirin first-pass metabolism in conjunction with ribavirin phosphorolysis.

On the other hand, although apparently less significant than that of the small intestine, our results also show the functional ability of the liver to metabolize ribavirin. This should be interpreted with caution, however, given that $TCONH_2$ levels remain very low in the rat livers after ribavirin oral administration, even though ribavirin and its phosphates are accumulated substantially.[15] This is unlikely to be due to the lack of PNP in the rat liver, since we have observed its abundant expression (unpublished observation). Therefore, it seems likely that, preferentially, ribavirin proceeds to the phosphorylation pathway rather than the phosphorolysis pathway once it enters a hepatocyte, as has been observed in several other cell types.[16] Collectively, even though the liver indeed expresses functional PNP, its role in ribavirin clearance currently remains inconclusive.

Given the important role of PNP in ribavirin metabolism, it is plausible that genetic variations in the *PNP* gene affect the ribavirin pharmacokinetic profile. However, in this study, we did not observe any significant PNP p.G51S effects on its ribavirin phosphorolysis activity *in vitro*, leading to the tentative understanding that special attention to the rs1049564 carriers is not necessary during ribavirin-based therapy. Nevertheless, several other mutations, including those responsible for PNP deficiency,[6] have been identified in the *PNP* gene, which indicates that it may be worthwhile to continue analysis of the *PNP* gene in order to identify genetic markers that would allow improved prediction of ribavirin pharmacokinetics and treatment responses.

In conclusion, our results indicate that the human small intestine is a key site for ribavirin phosphorolysis and that PNP is primarily involved in the metabolism. Based on these results, it is considered likely that the functional level of PNP is one of the factors governing ribavirin plasma concentration, thus eventually affecting treatment response. Although our results indicate no rs1049564 functionality in PNP's ribavirin phosphorolysis activity, further pharmacogenomic study, as well as biochemical characterization aimed at identification of variability in PNP functionality among individuals, can be expected to provide clinically important findings in ribavirin-based chronic hepatitis C therapy.

References

1) Dixit, N. M. and Perelson, A. S.: The metabolism, pharmacokinetics and mechanisms of antiviral activity of ribavirin against hepatitis C virus. *Cell. Mol. Life Sci.*, **63**: 832–842 (2006).
2) Iikura, M., Furihata, T., Mizuguchi, M., Nagai, M., Ikeda, M., Kato, N., Tsubota, A. and Chiba, K.: ENT1, a ribavirin transporter, plays a pivotal role in antiviral efficacy of ribavirin in a hepatitis C virus replication cell system. *Antimicrob. Agents Chemother.*, **56**: 1407–1413 (2012).
3) Tsubota, A., Hirose, Y., Izumi, N. and Kumada, H.: Pharmacokinetics of ribavirin in combined interferon-alpha 2b and ribavirin therapy for chronic hepatitis C virus infection. *Br. J. Clin. Pharmacol.*, **55**: 360–367 (2003).
4) Paroni, R., Del Puppo, M., Borghi, C., Sirtori, C. R. and Galli Kienle, M.: Pharmacokinetics of ribavirin and urinary excretion of the major metabolite 1,2,4-triazole-3-carboxamide in normal volunteers. *Int. J. Clin. Pharmacol. Ther. Toxicol.*, **27**: 302–307 (1989).
5) Preston, S. L., Drusano, G. L., Glue, P., Nash, J., Gupta, S. K. and McNamara, P.: Pharmacokinetics and absolute bioavailability of ribavirin in healthy volunteers as determined by stable-isotope methodology. *Antimicrob. Agents Chemother.*, **43**: 2451–2456 (1999).
6) Bzowska, A., Kulikowska, E. and Shugar, D.: Purine nucleoside phosphorylases: properties, functions, and clinical aspects. *Pharmacol. Ther.*, **88**: 349–425 (2000).
7) Wu, J. Z., Larson, G. and Hong, Z.: Dual-action mechanism of viramidine functioning as a prodrug and as a catabolic inhibitor for ribavirin. *Antimicrob. Agents Chemother.*, **48**: 4006–4008 (2004).
8) Tumini, E., Porcellini, E., Chiappelli, M., Conti, C. M., Beraudi, A., Poli, A., Caciagli, F., Doyle, R., Conti, P., *et al.*: The G51S purine nucleoside phosphorylase polymorphism is associated with cognitive decline in Alzheimer's disease patients. *Hum. Psychopharmacol.*, **22**: 75–80 (2007).
9) De Chaudhuri, S., Ghosh, P., Sarma, N., Majumdar, P., Sau, T. J., Basu, S., Roychoudhury, S., Ray, K. and Giri, A. K.: Genetic variants associated with arsenic susceptibility: study of purine nucleoside phosphorylase, arsenic (+3) methyltransferase, and glutathione S-transferase omega genes. *Environ. Health Perspect.*, **116**: 501–505 (2008).
10) Witte, D. P., Wiginton, D. A., Hutton, J. J. and Aronow, B. J.: Coordinate developmental regulation of purine catabolic enzyme expression in gastrointestinal and post-implantation reproductive tracts. *J. Cell Biol.*, **115**: 179–190 (1991).
11) Patil, S. D., Ngo, L. Y., Glue, P. and Unadkat, J. D.: Intestinal absorption of ribavirin is preferentially mediated by the Na^+-nucleoside purine (N1) transporter. *Pharm. Res.*, **15**: 950–952 (1998).
12) Stow, R. A. and Bronk, J. R.: Purine nucleoside transport and metabolism in isolated rat jejunum. *J. Physiol.*, **468**: 311–324 (1993).
13) He, Y., Sanderson, I. R. and Walker, W. A.: Uptake, transport and metabolism of exogenous nucleosides in intestinal epithelial cell cultures. *J. Nutr.*, **124**: 1942–1949 (1994).
14) Errasti-Murugarren, E., Pastor-Anglada, M. and Casado, F. J.: Role of CNT3 in the transepithelial flux of nucleosides and nucleoside-derived drugs. *J. Physiol.*, **582**: 1249–1260 (2007).
15) Miller, J. P., Kigwana, L. J., Streeter, D. G., Robins, R. K., Simon, L. N. and Roboz, J.: The relationship between the metabolism of ribavirin and its proposed mechanism of action. *Ann. N. Y. Acad. Sci.*, **284**: 211–229 (1977).
16) Page, T. and Connor, J. D.: The metabolism of ribavirin in erythrocytes and nucleated cells. *Int. J. Biochem.*, **22**: 379–383 (1990).

Drug Metab. Pharmacokinet. 29 (1): 1–2 (2014).

Editorial

Perspective of Humanized Mouse Models for Assessing PK/PD and Toxic Profile of Drug Candidates in Preclinical Study

Full text of this paper is available at http://www.jstage.jst.go.jp/browse/dmpk

The aim of preclinical studies is to evaluate the safety and pharmacological effect of new drug entities through *in vitro* and *in vivo* laboratory animal testing. However, the validity of animal testing to predict drug efficacy and safety in humans is not always guaranteed because of the existence of species differences between experimental animals and humans. Thus *in vitro* studies using human materials, such as human liver microsomes, human hepatocytes and liver slices, and recombinant human enzymes or transporters, have also been used in the case of ADME testing for predicting human drug metabolism and pharmacokinetics. Although results obtained from those *in vitro* methods are valuable, they alone are unlikely tell us how the variable processes of drug disposition will modulate the potency of the pharmacological activity of drugs in humans.[1] One of the ways to overcome the difficulties is to use humanized animal models.

Up to now, transgenic humanized mouse models have been developed for phase I enzymes (CYP1A1/1A2, CYP2A6, CYP2A13/2B6/2F1, CYP2C9, CYP2C18/2C19, CYP2D6, CYP2D6/3A4, CYPP2E1, CYP3A4, CYP3A7 and CYP3A4/3A5/3A7/3A43), and phase II enzymes (NAT2, UGT1A and UGT2B7) for the assessment of human drug metabolism, and xenobiotic receptors (AHR, PXR, CAR and PPAR α) for the assessment of gene activation.[2,3] As for transporters, transgenic humanized mouse models have been developed for ABCC2 and OATP1B1/1B3.[2] Moreover, an advanced humanized mouse model introducing multiple drug metabolizing enzymes and xenobiotic receptor genes has also been developed for the assessment of their interplay.[4]

In addition to genetically modified mouse models, chimeric mouse models with a humanized liver have been developed and applied for drug metabolism and pharmacokinetic studies. Although transgenic mouse models carry only one or two human genes, the chimeric model mice possess all phase I and II enzymes and transporters expressed in human liver. They produce human-specific drug metabolites, show induced expression of CYP enzymes in response to the administration of prototypical human-specific inducers, and show specific inhibition of various metabolic processes including CYP-mediated oxidations by prototypical inhibitors of human drug metabolism.[5,6]

Recently chimeric mice have been applied not only for ADME but also for pharmacodynamic studies. Drug candidates for viral hepatitis have been an ideal target of study, since chimeric mice can be exclusively infected with hepatitis B and C viruses. New types of direct-acting antiviral agents and their combinations were successfully evaluated by the chimeric mice, and the results mimicked those of human clinical trials.[7] Pharmacodynamic studies have also been performed for other hepatotropic infectious diseases using chimeric mice.[8] In addition, immunodeficient mouse models engrafted with human hematopoietic stem cells were used to study PK/PD properties of thrombopoietin receptor agonists.[9] Moreover, an immunodeficient mouse model engrafted with glucose-6-phosphae dehydrogenase deficient (G6PD) human red blood cells was applied to the assessment of the hemolytic toxicity of drugs.[10] This model could be a useful tool to test drugs for their potential to cause hemolytic toxicity in G6PD populations.

Genetically modified or transgenic humanized mouse models have also been applied for pharmacodynamics studies. Promyelocytic leukemia-retinoic acid receptor α transgenic mouse responded to all-trans retinoic acid therapy, suggesting that this mouse model could be a surrogate model to test therapeutic agents for human acute myelocytic leukemia.[9] A thrombopoietin receptor humanized mouse model was also used for a thrombopoietin receptor agonist to obtain an initial estimation of the concentration that would be required for therapeutic efficacy in clinics.[9]

At present, no regulations or guidelines are required for the use of humanized mouse models in preclinical study; however, the models would be a useful tool providing more precise information for human PK/PD and toxicity prediction.[7] As a matter of course, development of humanized mouse models is in the early stage and substantial efforts for functional improvement of human genes in the model should be required before practical use. Nonetheless, they may become an essential tool for preclinical studies by which the gap existing between experimental animals and humans could be bridged.[11]

References

1) Cheung, C. and Gonzalez, F. J.: Humanized mouse lines and their application for prediction of human drug metabolism and toxicological risk assessment. *J. Pharmacol. Exp. Ther.*, **327**: 288–299 (2008).
2) Scheer, N., Snaith, M., Wolf, C. R. and Seibler, J.: Generation and utility of genetically humanized mouse models. *Drug Discov. Today*, **18**: 1200–1211 (2013).
3) Kazuki, Y., Kobayashi, K., Aueviriyavit, S., Oshima, T., Kuroiwa, Y., Tsukazaki, Y., Senda, N., Kawakami, H., Ohtsuki, S., *et al.*: Trans-chromosomic mice containing a human CYP3A cluster for prediction of xenobiotic metabolism in humans. *Hum. Mol. Genet.*, **22**: 578–592 (2013).
4) Hasegawa, M., Kapelyukh, Y., Tahara, H., Seibler, J., Rode, A., Krueger, S., Lee, D. N., Wolf, C. R. and Scheer, N.: Quantitative prediction of human pregnane X receptor and cytochrome P450 3A4 mediated drug-drug interaction in a novel multiple humanized mouse line. *Mol. Pharmacol.*, **80**: 518–528 (2011).
5) Kitamura, S. and Sugihara, K.: Current status of prediction of drug disposition and toxicity in humans using chimeric mice with humanized liver. *Xenobiotica*, in press.
6) Kakuni, M., Yamasaki, C., Tachibana, A., Yoshizane, Y., Ishida, Y. and Tateno, C.: Chimeric mice with humanized livers: a unique tool for in vivo and in vitro enzyme induction studies. *Int. J. Mol. Sci.*, **15**: 58–74 (2013).
7) Peltz, G.: Can 'humanized' mice improve drug development in the 21st century? *Trends Pharmacol. Sci.*, **34**: 255–260 (2013).

8) Grompe, M. and Strom, S.: Mice with human livers. *Gastroenterology*, **145**: 1209–1214 (2013).
9) Sacca, R., Engle, S. J., Qin, W., Stock, J. L. and McNeish, J. D.: Genetically engineered mouse models in drug discovery research. *Methods Mol. Biol.*, **602**: 37–54 (2010).
10) Rochford, R., Ohrt, C., Baresel, P. C., Campo, B., Sampath, A., Magill, A. J., Tekwani, B. L. and Walker, L. A.: Humanized mouse model of glucose 6-phosphate dehydrogenase deficiency for in vivo assessment of hemolytic toxicity. *Proc. Natl. Acad. Sci. USA*, **110**: 17486–17491 (2013).
11) Foster, J. R., Lund, G., Sapelnikova, S., Tyrrell, D. L. and Kneteman, N. M.: Chimeric rodents with humanized liver: bridging the preclinical/clinical trial gap in ADME/toxicity studies. *Xenobiotica*, in press.

Kan CHIBA, Ph.D.

President of the JSSX
Graduate School of Pharmaceutical Sciences, Chiba University

OPEN ACCESS Freely available online

PLOS | ONE

Involvement of MAP3K8 and miR-17-5p in Poor Virologic Response to Interferon-Based Combination Therapy for Chronic Hepatitis C

Akihito Tsubota[1,2]*, Kaoru Mogushi[3], Hideki Aizaki[4], Ken Miyaguchi[3], Keisuke Nagatsuma[1,2], Hiroshi Matsudaira[1,2], Tatsuya Kushida[5], Tomomi Furihata[6], Hiroshi Tanaka[3], Tomokazu Matsuura[7]

1 Institute of Clinical Medicine and Research (ICMR), Jikei University School of Medicine, Kashiwa, Chiba, Japan, **2** Division of Gastroenterology and Hepatology, Kashiwa Hospital, The Jikei University School of Medicine, Kashiwa, Chiba, Japan, **3** Department of Bioinformatics, Medical Research Institute, Tokyo Medical and Dental University, Bunkyo-ku, Tokyo, Japan, **4** Department of Virology II, National Institute of Infectious Diseases, Shinjuku-ku, Tokyo, Japan, **5** National Bioscience Database Center, Japan Science and Technology Agency, Chiyoda-ku, Tokyo, Japan, **6** Laboratory of Pharmacology and Toxicology, Graduate School of Pharmaceutical Science, Chiba University, Chiba, Japan, **7** Department of Laboratory Medicine, Jikei University School of Medicine, Minato-ku, Tokyo, Japan

Abstract

Despite advances in chronic hepatitis C treatment, a proportion of patients respond poorly to treatment. This study aimed to explore hepatic mRNA and microRNA signatures involved in hepatitis C treatment resistance. Global hepatic mRNA and microRNA expression profiles were compared using microarray data between treatment responses. Quantitative real-time polymerase chain reaction validated the gene signatures from 130 patients who were infected with hepatitis C virus genotype 1b and treated with pegylated interferon-alpha and ribavirin combination therapy. The correlation between mRNA and microRNA was evaluated using *in silico* analysis and *in vitro* siRNA and microRNA inhibition/overexpression experiments. Multivariate regression analysis identified that the independent variables IL28B SNP rs8099917, hsa-miR-122-5p, hsa-miR-17-5p, and MAP3K8 were significantly associated with a poor virologic response. MAP3K8 and miR-17-5p expression were inversely correlated with treatment response. Furthermore, miR-17-5p repressed HCV production by targeting MAP3K8. Collectively, the data suggest that several molecules and the inverse correlation between mRNA and microRNA contributed to a host genetic refractory hepatitis C treatment response.

Citation: Tsubota A, Mogushi K, Aizaki H, Miyaguchi K, Nagatsuma K, et al. (2014) Involvement of MAP3K8 and miR-17-5p in Poor Virologic Response to Interferon-Based Combination Therapy for Chronic Hepatitis C. PLoS ONE 9(5): e97078. doi:10.1371/journal.pone.0097078

Editor: Wenyu Lin, Harvard Medical School, United States of America

Received December 6, 2013; **Accepted** April 14, 2014; **Published** May 12, 2014

Funding: This work was supported in part by Grants-in-Aid from the Ministry of Health, Labour and Welfare (Japan), the Ministry of Education, Culture, Sports, Science and Technology (Japan), and Clinical Research Funds from ICMR, the Jikei University School of Medicine. The funders had no role in study design, data collection and analysis, decision to publish, or preparation of the manuscript.

Competing Interests: The authors have declared that no competing interests exist.

* E-mail: atsubo@jikei.ac.jp

Introduction

Chronic hepatitis C (CH-C) caused by hepatitis C virus (HCV) infection is a major chronic liver disease worldwide, and it often develops into cirrhosis and hepatocellular carcinoma. Pegylated interferon alpha (peg-IFNα) and ribavirin (RBV) combination therapy is widely used to treat CH-C [1]. However, treatment fails in approximately 50% patients with HCV genotype 1. Of note, approximately 20–30% patients show null or partial response to the treatment. The introduction of nonstructural 3/4A protease inhibitors has improved the outcome for genotype 1 CH-C patients [1]. However, new antiviral agents increase the frequency and severity of adverse effects, are costly, have complex treatment regimens, and often result in viral resistance. Importantly, the outcomes of triple combination therapy are extremely poor in patients who showed null and partial response to previous peg-IFNα/RBV, compared to treatment-naïve patients and relapsers [1–3]. Furthermore, over 50% of null and partial responders, among all patients with a similar virologic response or viral kinetics, relapse after treatment cessation [2,3]. Collectively, these studies suggest a role of host genetics in treatment resistance.

Microarray applications in clinical medicine identified that numerous mRNAs and microRNAs (miRNAs) regulate complex processes involved in disease development. For example, hepatic mRNA expression of IFN-stimulated genes (ISGs, such as ISG15, OAS, IFI, IP10, and viperin) and IFN-related pathway genes (MX and USP18) correlate with responses to peg-IFNα/RBV combination therapy for CH-C [4–7]. However, few studies have examined global miRNAs alone [8]. Furthermore, mRNA and miRNA gene signatures and their interactions in treatment response have not been reported. miRNAs are evolutionarily conserved, small non-coding RNAs [9,10]. A single miRNA can regulate the expression of multiple target mRNAs and their encoded proteins by imperfect base pairing and subsequent mRNA cleavage/translational repression. Conversely, the expression of a single mRNA is often regulated by several miRNAs. As regulators of promotion or suppression of gene expression, miRNAs are involved in diverse biological and physiological processes, including cell cycle, proliferation, differentiation, and apoptosis. In addition to targeting endogenous mRNAs, miRNAs regulate the life cycle of viruses such as the Epstein-Barr virus,

HCV, and other oncogenic viruses by interacting with viral transcripts [11,12].

We investigated the differential expression profiles of mRNAs and miRNAs isolated from the liver tissues of untreated patients with HCV genotype 1b using microarray analysis. Expression profiles and their interactions were analyzed to identify the molecular signatures associated with treatment resistance.

Materials and Methods

Patient population, treatment, and liver tissue samples

During 2010 and 2011, 130 patients infected with HCV genotype 1b were treated weekly with 1.5 μg/kg of peg-IFNα-2b (MSD, Tokyo) and daily with 600–1000 mg RBV (MSD) [2,3] for 48 weeks at Jikei University Kashiwa-affiliated hospitals. Patients with undetectable serum HCV RNA at week 12 or later were recommended to extend the treatment to 72 weeks. All study participants provided informed written consent and materials for genetic testing and met the following criteria: (1) CH-C diagnosis confirmed by laboratory tests, virology, and histology; (2) genotype 1b confirmed by polymerase chain reaction (PCR)-based method; (3) absence of malignancy, liver failure, or other form of chronic liver disease; and (4) no concurrent treatment with any other antiviral or immunomodulatory agent. Liver specimens were obtained percutaneously before treatment, formalin-fixed, and paraffin-embedded for histological assessment [13]. A tissue section was stored in RNA*later* solution (Life Technologies, Carlsbad, CA). Total RNA containing mRNA and miRNA was isolated using the mirVana miRNA isolation kit (Life Technologies).

Sustained virological response (SVR) was defined as an undetectable serum HCV RNA level at 24 weeks after treatment completion. A null response was defined as a viral decline of $< 2\ \log_{10}$ IU/mL from baseline at treatment week 12 and detectable HCV RNA during treatment. A partial response was defined as a viral decline of $>2\ \log_{10}$ IU/mL from baseline at week 12, with no achievement of an undetectable HCV RNA level. Relapse was defined as an undetectable serum HCV RNA level at the end of treatment and viremia reappearance on follow-up examination [1]. Viral loads and the presence or absence of serum HCV RNA were evaluated using a qualitative PCR assay (Amplicor HCV version 2.0; Roche Diagnostics, Tokyo).

This study conformed to the provisions of the Declaration of Helsinki and Good Clinical Practice guidelines and was approved by the Jikei University Ethics Committee for Human Genome/Gene Analysis Research (No.21-093_5671).

mRNA microarray

Global mRNA expression analysis was performed using total RNA isolated from each sample [sustained virological responders (SVRs), $n=5$; relapsers, $n=3$; null responders, $n=4$] and the GeneChip Human Genome U133 Plus 2.0 Array (Affymetrix, Santa Clara, CA). Datasets were normalized by the robust multi-array analysis, using R 2.12.1 statistical software and the BioConductor package.

miRNA microarray

Global miRNA expression analysis was performed using total RNA isolated from the same samples used for mRNA expression analysis and the miRCURY LNA microRNA Array series (Exiqon, Vedbaek, Denmark). Total RNA was labeled with Hy3 and hybridized to slides that contained capture probes targeting all human miRNAs registered in the miRBASE 14.0. miRNA microarray datasets were normalized by quantile normalization using R statistical software.

Differential gene expression according to treatment response

The limma package from BioConductor software (under R statistical software) was used to calculate moderated t-statistics (based on the empirical Bayes approach) to identify mRNA or miRNA differentially expressed between the SVR/relapser group and null/partial responder group. Because of multiple hypothesis testing, p values were adjusted by the Benjamini-Hochberg false discovery rate (FDR) method.

Hierarchical cluster analysis

Up- and down-regulated probe sets were analyzed by hierarchical clustering using R statistical software. Pearson's correlation coefficients were used to calculate a matrix similarity score among the probe sets. The complete linkage method was used for agglomeration. Heat maps were generated from significant differentially expressed probe sets.

Quantitative real-time PCR for mRNA

To validate microarray results and to confirm the observed differences in the mRNA expression levels in a quantitative manner, each sample was subjected to reverse transcription (RT)-PCR and quantitative real-time RT-PCR (qPCR) in triplicate. After cDNA synthesis, target genes were amplified in PCR mixtures that contained TaqMan Universal PCR Master Mix (Life Technologies) and TaqMan probes designed with the Universal Probe Library Assay Design Center (http://www.roche-applied-science.com/sis/rtpcr/upl/adc.jsp). Target gene expression levels in each sample were normalized to the expression of the housekeeping gene of 18S rRNA and the corresponding gene of one null responder.

Quantitative real-time PCR for miRNA

cDNA was synthesized from aliquots of the isolated total RNA using the TaqMan MicroRNA Reverse Transcription kit (Life Technologies) including RT primers designed with miRNA-specific stem-loop structures according to manufacturer's protocol. miRNA expression levels were quantified with the TaqMan MicroRNA assay (Life Technologies) in triplicate. Target gene expression levels were normalized in each sample to the expression of the endogenous gene RNU48 and the corresponding gene of one null responder.

miRNA target prediction

Up- and down-regulated miRNAs with a fold change of >1.2 and $p<0.005$ (FDR<0.15) between two groups (SVRs/relapsers *vs* null responders) in the microarray analysis were subjected to the *in silico* prediction of mRNA targets for miRNA using MicroCosm Targets, miRanda, PicTar, PITA, and TargetScan algorithms. Predicted mRNA targets were analyzed further if they met the following criteria: (1) fold change of >1.5 and $p<0.003$ (FDR$<$ 0.35) in mRNA microarray results; (2) inverse correlation (negative correlation coefficient) between miRNA and mRNA in mRNA and miRNA microarray results; and (3) qPCR-validated microarray results. Kyoto Encyclopedia of Genes and Genomes (KEGG) Pathways, Agilent Literature Search 3.0.3 beta, and Cytoscape 3.0.2 were used to identify the significance of candidates in gene regulatory networks.

Cell culture

The human hepatoma cell line Huh7.5.1 (a gift from Professor Francis Chisari, Scripps Research Institute, La Jolla, CA) was maintained in Dulbecco's modified Eagle's medium containing 10% fetal bovine serum [14]. Cell culture-produced HCV (HCVcc) were harvested from JFH1-transfected Huh7.5.1 as previously described [15].

Plasmids and siRNAs

The siRNAs targeting MAP3K8 were siRNA1, 5′-uucgucuuuauaucuugugtt-3′; siRNA2, 5′-uguugcuagguuuaauauctt-3′; siRNA3, 5′-aucuugugccaaguauacctt-3′; and scrambled negative control siRNA to siRNA1 (Sigma-Aldrich, St. Louis, MO). The expression and inhibitor plasmids of hsa-miR-17-5p and control plasmids were purchased from GeneCopoeia (Rockville, MD).

HCV core antigen measurements and cell viability

The HCV core antigen concentrations in filtered culture medium and cell lysates of infected cells were measured with the Lumipulse Ortho HCV antigen kit (Ortho Clinical Diagnostics, Tokyo). Cell viability was analyzed using the CellTiter-Glo Luminescent Cell Viability Assay (Promega, Madison, WI).

Transfection

Cells were seeded into a 24-well plate and transfected with siRNAs and plasmids using Lipofectamine RNAiMAX (Invitrogen, San Diego, CA) and TransIT-LT1 (Mirus, Madison, WI), respectively.

Luciferase reporter assay

The MAP3K8 3′UTR segment containing the putative miR-17-5p target sites was subcloned into the pGL3 reporter plasmid (Promega). A mutant construct was also generated by PCR-based mutagenesis using mutagenic primers. The luciferase reporter and hsa-miR-17-5p expressing or mock plasmids were co-transfected with the *Renilla* luciferase transfection control plasmid. Luciferase reporter activity was measured 48 hours after transfection with the Dual-Luciferase Reporter Assay System (Promega).

Western blot

Liver samples were sonicated in lysis buffer. Lysate aliquots were separated by SDS-polyacrylamide gel electrophoresis and transferred onto a nitrocellulose membrane. Membranes were incubated with primary antibodies against MAP3K8 (ab70853, Abcam, San Diego, CA) and β-actin (EP1123Y, Abcam). Membranes were incubated with horseradish peroxidase-conjugated secondary antibodies. Immunoreactivity was detected with reagents (GE Healthcare Life Sciences, Piscataway, NJ). Images were scanned and band intensities quantified with Image J.

IL28B and ITPA single nucleotide polymorphism (SNP) genotyping

Genomic DNA was extracted from whole blood using the MagNA Pure LC and the DNA Isolation Kit (Roche Diagnostics). The IL28B rs8099917 and rs12979860 [16,17] and ITPA exon 2 rs1127354 [18] genetic polymorphisms were genotyped by real-time detection PCR with the TaqMan SNP Genotyping Assays.

Statistical analysis for factors associated with null/partial response

The chi-square, Fisher's exact, Student's *t*, and the Mann–Whitney two-tailed tests were used to compare frequencies in categorical data or differences in continuous data between two groups. Significant independent factors associated with null/partial responses were identify with multiple logistic regression analysis using the SPSS statistical package for Windows, version 17.0 (IBM SPSS, Chicago, IL). A p value of <0.05 was considered statistically significant.

Results

Patient profiles and treatment response

Among the 130 patients, 62 (48%) achieved SVR, 36 (28%) relapsed, and six (5%) and 26 (20%) showed partial and null response, respectively. Patients were divided into an SVR/relapser group and a null/partial responder group. Table S1 compares the baseline characteristics of the two groups. Patients with elevated serum gamma glutamyl transpeptidase and decreased albumin concentrations were more likely to experience a null/partial response. The IL28B rs8099917 TG and rs12979860 CT variants were more likely to be null/partial responders compared with TT and CC genotypes, respectively.

mRNAs associated with treatment response

mRNA microarray data were deposited into the NCBI Gene Expression Omnibus (GEO) (http://www.ncbi.nlm.nih.gov/geo/), accession number GSE42697. The cut-off criteria for fold change >1.5 and $p<0.003$ identified 39 up-regulated and 17 down-regulated annotated probe sets in null responders (Data S1). The up-regulated genes were associated with transcription, translation, cell cycle, phosphorylation, signal transduction, immune response, RNA splicing/mRNA processing, and viral reproduction. The down-regulated genes were associated with xenobiotic/small molecule/lipid metabolic and oxidation–reduction processes. Hierarchical clustering of mRNAs and samples showed that samples from SVRs and relapsers clustered to form a group different from the null responders (Fig. S1). To validate the microarray results, qPCR was performed for all significant differentially expressed genes. The expression levels of MAP3K8 (mitogen-activated protein kinase kinase kinase 8, $p=5.24\times10^{-7}$), TMEM178 (transmembrane protein 178, $p=7.31\times10^{-6}$), PSME4 (proteasome activator subunit 4, also known as *PA200*, $p=2.43\times10^{-4}$), and EIF3B (eukaryotic translation initiation factor-3B, $p=3.16\times10^{-6}$; Fig. 1) were significantly increased in null/partial responders compared with those in SVRs/relapsers. TMEM178 is a multi-pass membrane protein and PSME4 is a nuclear protein that activates the proteasome and is important for oxidative-stress adaptation. EIF3B is involved in protein translation/synthesis and interacts with the HCV IRES and the 40S ribosomal subunit.

miRNAs associated with treatment response

miRNA microarray data were deposited into the NCBI GEO, accession number GSE45179. The cut-off criteria for fold change >1.2 and $p<0.005$ identified 111 down-regulated and 76 up-regulated miRNAs in null responders (Data S2). Hierarchical two-dimensional clustering showed that distinct patient groups clustered into two distinct groups (Fig. S2). Bioinformatic analysis predicted target genes of the differentially expressed miRNAs. The hypothetical target genes should be MAP3K8, TMEM178, PSME4, and EIF3B. Furthermore, these miRNAs and mRNAs must have an inverse correlation between mRNA and miRNA microarray data. The microRNAs that satisfied the requirements were as follows: hsa-let-7g* and hsa-miR-17-5p, -20b, -297, -374b, -494, -602, -668, and -1297 for MAP3K8; hsa-miR-106b* and -122-5p for TMEM178; and hsa-miR-492 and -675-5p for PSME4. No corresponding miRNA was identified for EIF3B.

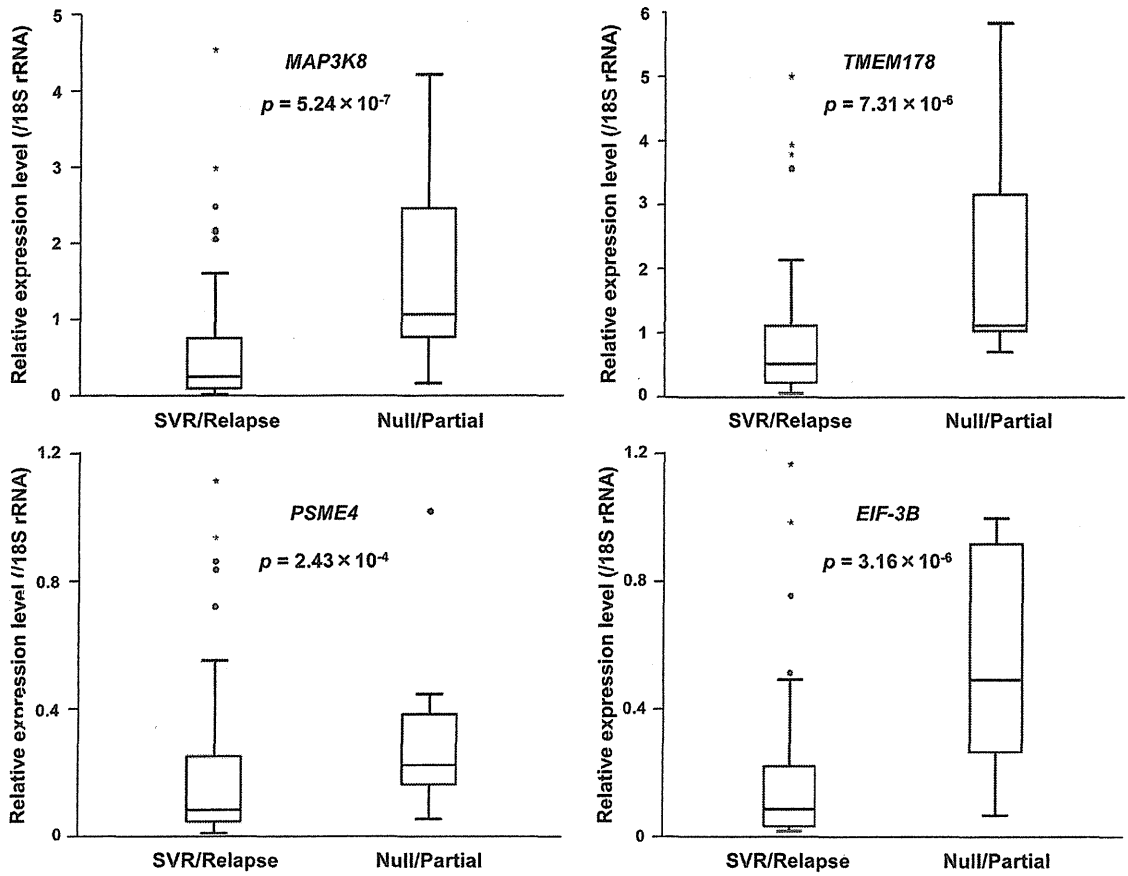

Figure 1. Validation of differentially expressed mRNAs by qPCR analysis. The expression levels of four mRNAs were significantly higher in null/partial responders than in SVRs/relapsers. Assays for each sample were performed in triplicate. All *p*-values were calculated using the Mann–Whitney test.
doi:10.1371/journal.pone.0097078.g001

Stem-loop-based qPCR was performed to confirm the reliability of the miRNA microarray results and the inverse correlation between miRNA and mRNA. The expression levels of hsa-miR-122-5p ($p = 2.75 \times 10^{-8}$), hsa-miR-675-5p ($p = 1.00 \times 10^{-5}$), and hsa-miR-17-5p ($p = 1.73 \times 10^{-8}$) were significantly lower in null/partial responders than in SVRs/relapsers (Fig. 2).

Independent variables associated with treatment response

Multiple logistic regression analysis of variables that were significant in univariate analysis identified that rs8099917 [$p = 3.67 \times 10^{-3}$, odds ratio (OR) = 7.51, 95% confidence interval (CI) = 2.14–29.27], hsa-miR-122-5p ($p = 5.60 \times 10^{-4}$, OR = 0.11, 95% CI = 0.03–0.38), hsa-miR-17-5p ($p = 2.02 \times 10^{-4}$, OR = 0.56, 95% CI = 0.41–0.76), and MAP3K8 ($p = 8.58 \times 10^{-3}$, OR = 2.86, 95% CI = 1.31–6.25) were significantly associated with null/partial response. Importantly, *in silico* analysis and microarray data suggested that increased miR-17-5p could cause MAP3K8 reduction. In fact, an inverse correlation was observed between MAP3K8 mRNA and miR-17-5p ($r = -0.592$, $p = 4.31 \times 10^{-3}$). MAP3K8 is closely linked to genes associated with cell proliferation, inflammation, and apoptosis (Fig. S3) and is associated with the miR-17 cluster family (Fig. S4).

MAP3K8 contributes to HCV production

siRNA transfection in HCVcc-infected cells was performed to assess the influence of MAP3K8 mRNA and protein on HCV production (Fig. 3A). miR-17-5p levels were significantly increased (Fig. 3B) while supernatant HCV core antigen levels were significantly decreased following transfection of the siRNAs (Fig. 3C). However, the HCV core antigen levels in cell lysates were not changed (Fig. 3C). Taken together, these findings suggested that MAP3K8 repressed miR-17-5p and contributed to the production (e.g. release and assembly) of HCV. *In vivo*, MAP3K8 protein expression levels were significantly increased in null/partial responders compared with those in SVRs/relapsers ($p = 2.43 \times 10^{-5}$).

Hsa-miR-17-5p regulates HCV production by targeting MAP3K8

Changes in MAP3K8 and HCV core antigen levels were evaluated by hsa-miR-17-5p inhibition and overexpression in HCVcc-infected cells. miR-17-5p inhibition increased MAP3K8 mRNA and protein levels (Fig. 4A and 4B, left). In contrast, miR-17-5p overexpression decreased MAP3K8 mRNA and protein levels (Fig. 4A and 4B, right). Interestingly, miR-17-5p inhibition increased, whereas miR-17-5p overexpression decreased HCV core antigen levels in both supernatants and cell lysates (Fig. 4C).

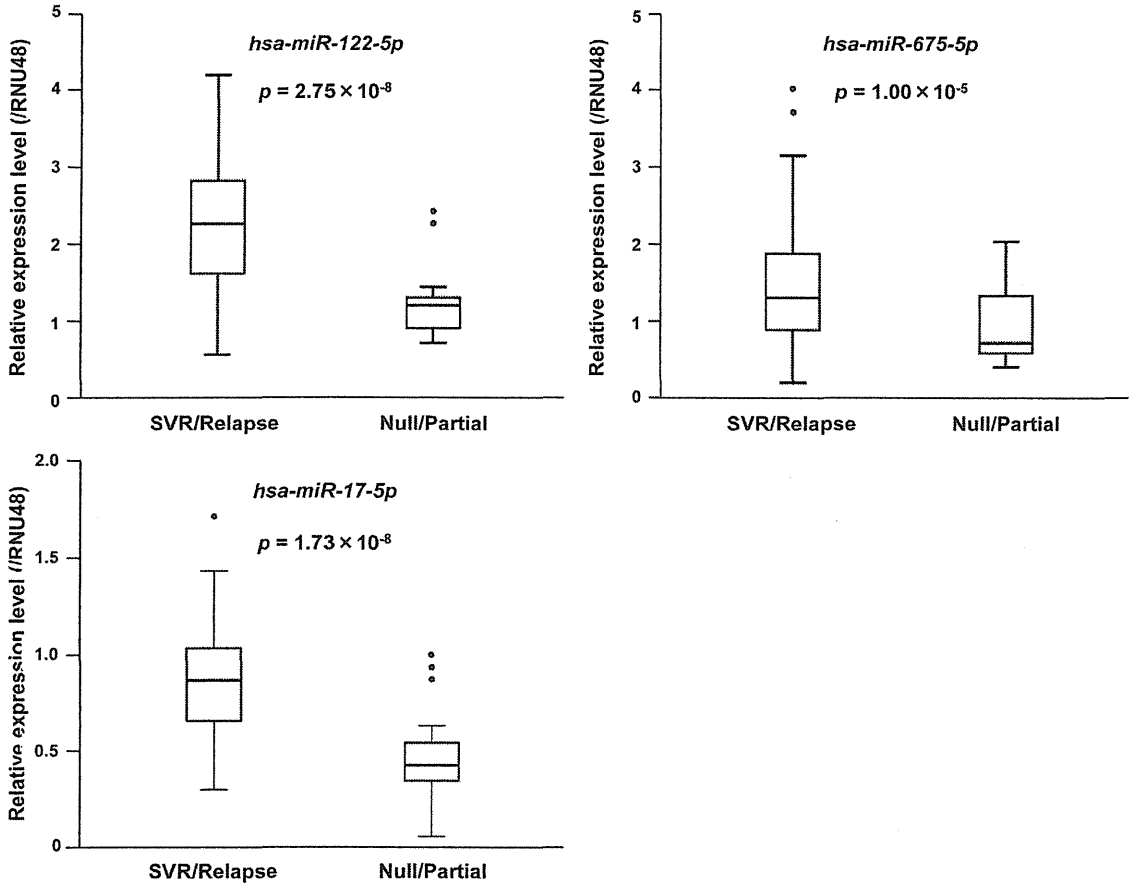

Figure 2. Validation of differentially expressed miRNAs by qPCR analysis. The expression levels of three miRNAs were significantly higher in null/partial responders than in SVRs/relapsers. Assays for each sample were performed in triplicate. All *p*-values were calculated using the Mann–Whitney test.
doi:10.1371/journal.pone.0097078.g002

Taken together, these results suggested that miR-17-5p regulated the production of HCV by targeting MAP3K8 mRNA. Luciferase reporter assays showed that miR-17-5p overexpression decreased the luciferase activity of the wild-type MAP3K8 3′UTR reporter construct, whereas co-transfection with the mutant MAP3K8 3′UTR construct or mock had no effect (Fig. 5), suggesting that miR-17-5p targeted the MAP3K8 3′UTR and antagonized MAP3K8 protein expression.

Discussion

This study showed close linkage between mRNA and miRNA signatures in CH-C treatment outcomes using global expression profiling analyses. To confirm the findings, this cohort was randomly divided into derivation and confirmatory groups. The derivation group results were similar to those described above and reproducible in the confirmatory group (data not shown). Subsequently, we attempted to compare our findings with registered patient data obtained from independent cohorts comprising either Asian or non-Asian subjects. However, comparisons were not possible because most mRNA or miRNA microarray studies had a small sample size, limited information, unregistered data, and/or findings that were not validated in an independent cohort [4–7,11,19–21]. To our knowledge, our study was the first to investigate the correlation between mRNA and miRNA in treatment response using global gene expression analysis and *in vitro* experiments. Such gene signature identification can improve the accuracy of treatment outcome predictions, independent of known strong predictors.

Pretreatment hepatic ISG levels are higher in non-SVRs/non-relapsers than in SVRs/relapsers [4–7]. The poor ISG response of non-SVRs with further exogenous IFN may contribute to treatment failure [5,6]. Because patient groups with different response categories differ in their innate IFN response to HCV infection; poor responders may have adopted a different equilibrium in their innate immune response to HCV [4,6]. As per multivariate regression analysis, however, IL28B SNPs may diminish the significance of hepatic ISGs as treatment predictors because hepatic ISG expression is associated with IL28B SNPs [7,19]. Conversely, hepatic ISGs were reported to be stronger predictors compared with IL28B SNPs [20]. Although our gene set enrichment analysis (data not shown) also showed that hepatic ISG expression levels were generally higher in null/partial responders than in SVRs/relapsers, the differences were not large enough to be ranked in a higher order and/or to reach statistical significance in expression profiling and validation analyses (Data S3). These variations among studies may be caused by different and heterogeneous patient characteristics, including HCV geno-

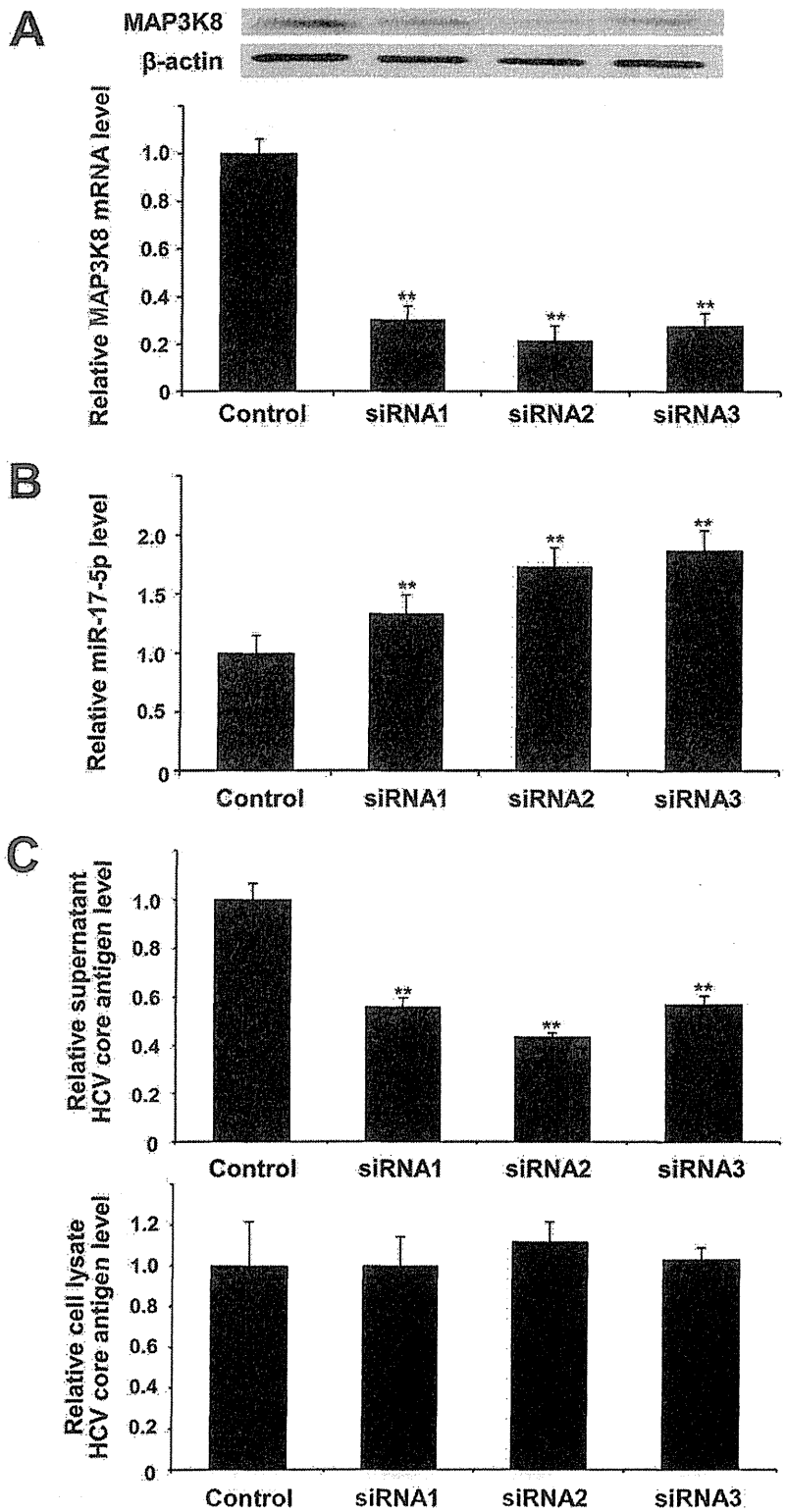

Figure 3. Transfection of Huh7.5.1 cells with siRNAs against MAP3K8. (**A**) Transfection of Huh7.5.1 cells with siRNAs against MAP3K8 significantly decreased intracellular MAP3K8 mRNA levels, (**B**) increased intracellular hsa-miR-17-5p levels, and (**C**) decreased HCV core antigen levels in the supernatant, and had no effect on those in cell lysate. Bars indicate the means of three independent experiments and the error bars indicate standard deviations. All *p*-values were calculated using two-tailed Student's *t*-test. $^{**}p<0.001$ compared with controls.
doi:10.1371/journal.pone.0097078.g003